Anisotropy of the Magnetoresistance Hysteresis in the Granular Superconductor Y-Ba-Cu-O at Different Magnetic-Field and Transport-Current Orientations

Balaev D.A.[1,2], Semenov S.V.[1,2], and Pochekutov M.A.[2]
[1] - Kirensky Institute of Physics, Federal Research Center KSC SB RAS, Krasnoyarsk, 660036 Russia.
[2] - Siberian Federal University, Krasnoyarsk, 660041 Russia

e-mail: dabalaev@iph.krasn.ru

Abstract. Dissipation in granular high-temperature superconductors (HTSs) during the passage of macroscopic transport current $\boldsymbol{j}$ is mainly determined by carrier tunneling through the intergrain boundaries (Josephson junctions). In the presence of external magnetic field $\boldsymbol{H}$, it is necessary to take into account the significant magnetic flux compression, which can lead to the situation when the effective field B_{eff} in the intergrain boundaries exceeds the external field by an order of magnitude. This is observed as a wide hysteresis of the field dependence of magnetoresistance $R(H)$. In this study, we investigate the R(H) hysteresis evolution in granular 1-2-3 HTSs at different $\boldsymbol{j}$–$\boldsymbol{H}$ orientations. The magnetic flux compression significantly affects the magnetoresistance and its hysteresis for both perpendicular ($\boldsymbol{H} \perp \boldsymbol{j}$) and parallel ($\boldsymbol{H} \parallel \boldsymbol{j}$) orientations. The obtained experimental data on the $R(H)$ hysteresis at the arbitrary angles $\theta = \angle \boldsymbol{H}, \boldsymbol{j}$ are explained using the approach developed for describing the magnetoresistance hysteresis in granular HTSs with regard to the magnetic flux compression and the model representations proposed by Daghero et al. [Phys. Rev. B **66** (13), 11478 (2002)]. A concept of effective field in the intergrain medium explains the well-known anisotropy of magnetotransport properties of granular HTSs.

1. Introduction

Study of the magnetotransport properties of superconductors yields information useful for establishing the mechanisms responsible for pinning of Abrikosov vortices. In the general case, the magnetoresistance is determined using the Arrhenius expression[1]

$$R \sim \exp(-U_P(H, T, j) / k_B T), \quad (1)$$

where $U_P(H, T, j)$ is the dependence of the pinning potential on magnetic field, temperature, and transport current and k_B is the Boltzmann constant. The situation is complicated at the dissipation in granular high-temperature superconductors (HTSs). These objects represent random systems of superconducting grains, where the dissipation occurs mainly in the subsystem of intergrain boundaries, which are the areas with the suppressed superconducting properties behaving as weak links (Josephson junctions) for tunneling of superconducting current carriers[2,3].

In the highly anisotropic HTSs, e.g., Bi-2223 and Bi-2212, it is necessary to take into account the preferred current flowing within grains (crystallites) along the *a*-*b* planes. This is made in the so-called break-wall [4] (railway) switch[5,6] models, which explain the experimentally observed critical current anisotropy in the Bi-2223 and Bi-2212 tapes at different magnetic field orientations relative to the *a*-*b* planes of grains. The Y- and La-based HTSs (YBCO and LSCO) have, as is known, a much weaker anisotropy of the superconducting properties than the Bi-based HTSs. However, even the non-textured YBCO and LSCO (as well as non-textured Bi-2223) bulk granular HTSs exhibit the anisotropy of magnetotransport properties at different mutual directions of magnetic field $\boldsymbol{H}$ and transport current $\boldsymbol{j}$ (hereinafter, vector $\boldsymbol{j}$ denotes the macroscopic transport current direction).

Although the above-mentioned anisotropy was found soon after the discovery of HTS[7-11], the model representation of the magnetoresistance anisotropy in such a random system as a granular superconductor was proposed much later[12]. Daghero et al. took into account that the magnetic field in the intergrain spacings is determined not only by the external field, but also by the fields induced by screening currents flowing over the superconducting grain surface (the Meissner effect). This allowed the behavior of the anisotropy parameter $R(\boldsymbol{H} \parallel \boldsymbol{j})/R(\boldsymbol{H} \perp \boldsymbol{j}) < 1$ in the yttrium HTS system in weak magnetic fields to be explained.

Another specific feature of granular superconductors is the hysteretic-field dependence of magnetoresistance $R(H)$[13-26], which is explained by the effect of magnetic moments of superconducting grains on the effective field in the intergrain medium. The aim of this study was to develop the model of the

behavior of a granular HTS in the external field and explain the magnetoresistance hysteresis anisotropy at arbitrary angles $\theta = \angle \boldsymbol{H}, \boldsymbol{j}$, in particular, determine the degree of magnetic flux compression in the intergrain medium. The model was confirmed using a technique for determining the effective field in the intergrain medium directly from the experimental data on magnetization and magnetoresistance [27-29].

Since the yttrium HTS sample used in the measurements at the liquid nitrogen temperature exhibits the properties typical of such materials, the results obtained can be generalized to, at least, granular 1-2-3 HTS materials. The model (Section 3) that explains the hysteretic behavior of magnetoresistance is confirmed by the data for the yttrium HTS composite. This sample can be used as a reference, since the Josephson coupling between HTS grains in it was purposefully weakened by adding a non-superconducting component and the critical current was significantly reduced[24,25,30]. This allows one to perform the magnetoresistance measurements at the liquid helium temperature at weak measuring currents.

2. Experimental

The bulk $YBa_2Cu_3O_7$ (YBCO) HTS sample for the magnetoresistance hysteresis measurements at different $\boldsymbol{H}$ and $\boldsymbol{j}$ orientations was prepared by a standard solid-state reaction technique. X-ray analysis revealed only the 1-2-3 structure reflections. According to the scanning electron microscopy data, the average grain size was 6 μm. Above T_C (90.5 K), the metal-type $R(T)$ dependence typical of such systems was observed.

The data presented in Section 3 were obtained using a composite consisting of 77.5 vol.% of $Y_{0.75}Lu_{0.25}Ba_2Cu_3O_7$ and 22.5 vol.% of CuO, hereinafter referred to as the YBCO *composite*. The sample fabrication procedure included [30] (i) mixing of initial components (finished HTS and copper oxide) with subsequent pressing and (ii) joint annealing at $T = 900^0$C for 5 min with subsequent exposure at 400^0C for 4 h in another furnace. This process yields bulk samples with HTS grains doped with oxygen in the optimal concentration (the transition temperature does not decrease) [26]; the Josephson coupling in the subsystem of intergrain boundaries is purposefully weakened.

The transport measurements were performed on the samples with typical sizes of about $1\times1\times(5\div7)$ mm^3. The $R(H)$ dependences were measured by a standard four-probe method. The transport current was applied along the sample length $\boldsymbol{L}$. The $R(H)$ dependence for the YBCO-*composite* sample was measured in the perpendicular configuration ($\boldsymbol{L}\perp\boldsymbol{H}$) at a transport current of 5 mA and a temperature of $T = 4.2$ K (the sample was in the helium heat-exchange atmosphere). During the measurements of $R(H)$ dependences, the YBCO sample was in the liquid nitrogen medium and the current was $I = 30$ mA. The external field was induced by an electromagnet, which allowed us to determine the transport characteristics at the arbitrary angles $\theta = \angle \boldsymbol{H}, \boldsymbol{j}$. After zero-field cooling (ZFC), the external field was increased to its maximum values (±500 Oe). Below, we analyze the forward and reverse branches of the obtained hysteretic dependences.

The magnetic measurements were performed on a vibrating sample magnetometer on the samples used in the magnetotransport measurements.

3. Justification of the model

3.1. Magnetoresistance hysteresis

We limit the consideration to the case when the dissipation only occurs in the intergrain medium. This suggests that under the experimental conditions the inequality $J_{C\_grain}(H) >> J_{C\ intergrain}(H)$ (J_C is the critical current in an applied magnetic field) is valid. The YBCO HTSs satisfy this inequality at liquid nitrogen temperatures in fields of, at least, up to ~ 50 kOe[31, 32].

To explain the $R(H)$ hysteresis observed in granular superconductors, it is necessary to take into account that the magnetic field in the intergrain spacings is a superposition of the external field and the field induced by magnetic moments of superconducting grains. Obviously, the magnetic moment $\boldsymbol{M}_G$ of a grain is proportional to the magnetic moment $\boldsymbol{M}$ of a sample. Then, the field dependence of $\boldsymbol{M}_G$ is similar to the experimental $M(H)$ dependence. Figure 1a shows the hysteretic $M(H)$ dependence for the YBCO-*composite* sample. The shape of $M(H)$ hysteresis loop is consistent with the critical state model[33].

In the areas of increasing ($H = H_{inc}$) and decreasing ($H = H_{dec}$) external field in Fig. 1a, the lines of magnetic induction $\boldsymbol{B}_{ind}$ of the grain magnetic moments are schematically shown. The resulting effective field $\boldsymbol{B}_{eff}$ in the intergrain spacing is the superposition of external field $\boldsymbol{H}$ and $\boldsymbol{B}_{ind}$:

$$\boldsymbol{B}_{eff} = \boldsymbol{H} + \boldsymbol{B}_{ind}. \quad (2)$$

In Figs.1a, 2, and 3, we introduced the z axis parallel to the magnetic field H and oriented upwards. It can be seen in Fig.1a that the contributions from $\boldsymbol{M}_G$ to the z component of the field in the intergrain medium have

different signs at the increasing ($M_z < 0$, $\boldsymbol{M}_{G,z} < 0$, and $\boldsymbol{B}_{ind} \parallel \boldsymbol{H}_{inc}$) and decreasing external field ($M_z > 0$, $\boldsymbol{M}_{G,z} > 0$, and $\boldsymbol{B}_{ind}$ is antiparallel to $\boldsymbol{H}_{dec}$).

Then, the resulting effective field $\boldsymbol{B}_{eff,z}$ will be stronger at the increasing field, i.e., $B_{eff,z}(H = H_{inc}) > B_{eff,z}(H = H_{dec})$ at $H_{inc} = H_{dec}$. In turn, the $R(H)$ dependence is determined by expression (1), where the external field should be replaced by the effective field in the intergrain medium ($B_{eff} \rightarrow H$). This leads to the $R(H)$ hysteresis (see Fig. 1b, ($R(H = H_{inc}) > R(H = H_{dec})$).

3.2. Magnetic flux compression in the intergrain medium

Obviously, the field induced by $\boldsymbol{M}_G$ in the intergrain medium (Figs. 1a and 2a) is nonuniformly distributed. It would be reasonable to make the following assumption: the field $\boldsymbol{B}_{ind}$ induced by $\boldsymbol{M}_G$ is proportional to the magnetic moment of the sample, since the total magnetic moment of the sample is a superposition of magnetic moments of grains[33] and the contribution of the intergrain medium is insignificant[34-36]. Then, taking into account carrier tunneling through the intergrain boundaries, we can use the numerical value of the z component of $\boldsymbol{B}_{ind}$ in the intergrain medium

$$B_{ind,z} = -4\pi M_z \alpha. \quad (3)$$

The proportionality factor α in Eq. (3) characterizes crowding of the magnetic flux lines in the intergrain spacings. Certainly, when the intergrain distance is sufficiently large (Fig.2a), the α value will by similar to the demagnetizing factor of a grain. However, if we bring two grains closer to one another (Fig. 2b) to obtain the intergrain distance typical of granular materials (about the coherence length, i.e., ~ 1−2 nm for YBCO[3]), then the magnetic induction lines in the spacing between two grains will be essentially crowded[12,15] and, consequently, the parameter α will increase. Note that the spacing between neighboring grains in the schematic shown in Fig. 2b (see also insets in Fig.1a, and Figs. 3a and 3b) is significantly enlarged (this spacing is much smaller than the grain size).

To estimate the α value, we proposed the approach[27] in which the $R(H)$ and $M(H)$ hysteretic dependences are compared and the magnetoresistance hysteresis width $\Delta H = H_{dec} - H_{inc}$ under the condition $R(H_{inc}) = R(H_{dec})$ is considered (Fig. 1b). The equality of magnetoresistances at the points H_{dec} and H_{inc} of the $R(H)$ hysteretic dependence suggests that the effective fields (Eq. (2)) at these points are also equal, since the R value is determined by Eq. (1). Taking into account the sign of magnetic moment of the sample with respect to the z component (see Fig. 1a) and Eq. (3), we can rewrite Eq. (2) in the form

$$B_{eff,z}(H) = H_z - 4\pi M_z(H_z)\alpha. \quad (4)$$

Substituting sequentially $H = H_{dec}$ and $H = H_{inc}$ in (4) and subtracting one expression from the other, we arrive at

$$\Delta H = H_{dec} - H_{inc} = \alpha\, 4\pi\, [M(H_{inc}) - M(H_{dec})] \quad (5)$$

(index z is omitted). It this expression, we put α = const; i.e., assumed the parameter α to be magnetic field-independent ($\alpha \neq f(H)$). The horizontal segment in Fig. 1b corresponds to the ΔH value at H_{dec} = 16.5 kOe; the points indicated in the experimental $M(H)$ dependences (Fig.1a) correspond to the «magnetic state» of the sample at $H = H_{dec}$ and $H = H_{inc}$.

Expression (5) can be used to analyze the field width of the magnetoresistance hysteresis using the experimental $R(H)$ and $M(H)$ dependences, since the parameter ΔH is independent of the transport current in its wide range[23-26,37]. As was shown by different measurements, the α value is about 10 and more[27-29], which is indicative of crowding of the magnetic flux lines in the intergrain medium (Fig. 2b) due to the small grain boundary thickness as compared with the grain size.

3.3. Effective field in the intergrain media at different $\theta = \angle \boldsymbol{H}, \boldsymbol{j}$

In the classical Bardeen–Stephen approach, the magnetoresistance dependence on the angle $\theta = \angle \boldsymbol{H}, \boldsymbol{j}$ for the type-II superconductors is proportional to $\sin^2\theta$ [38,39]. The idealized picture of microscopic trajectories of current $\boldsymbol{I}$ for the orientation $\boldsymbol{H} \parallel \boldsymbol{j}$ (i.e., $\boldsymbol{B}_{eff,z} \parallel \boldsymbol{I}$) is presented in Fig. 3a; if the normal $\boldsymbol{n}$ to the intergrain boundary plane S is strictly parallel to the external field (i.e., $\boldsymbol{n} \parallel \boldsymbol{I}$), then there is no magnetic flux crowding in the region of carrier tunneling. In this ideal case, the flux crowding will not influence carrier tunneling through the intergrain boundary. On the contrary, in the case illustrated in Fig. 3b, the normal $\boldsymbol{n}$ is perpendicular to both the external field $\boldsymbol{H}$ and induced field $B_{ind,z}$; therefore, carriers are forced to tunnel through the region of the maximum flux crowding. Thus, the maximum effect of flux compression on the magnetoresistance is expected at the angle $\theta = \pi/2$.

At arbitrary angles θ (Fig. 3c), the tunneling processes will be affected by the projections of vectors $\boldsymbol{B}_{ind}$ and $\boldsymbol{H}$ onto the $\boldsymbol{s}$ axis. We introduce the $\boldsymbol{s}$ axis, which is perpendicular to $\boldsymbol{n}$ (i.e., parallel to the intergrain boundary plane S) and lies in the plane formed by the vectors $\boldsymbol{H}$ and $\boldsymbol{I}$ (Figs. 3b and 3c). Since we have $\boldsymbol{n} \parallel \boldsymbol{I}$,

$\theta = \angle \boldsymbol{H}, \boldsymbol{I}$, and $\theta = \angle \boldsymbol{n}, z$ ($\boldsymbol{n} \perp \boldsymbol{s}$), at arbitrary angle θ the magnetoresistance is determined by the components $B_{ind,z} \sin\theta$ and $H \sin\theta$. A similar approach was used in[12] (see Ref. 40). Thus, we can write the expression for the effective field projection (Eq. (4)) of $B_{eff}(H)$ onto the $\boldsymbol{s}$ axis:

$$B_{eff,s}(H) = [H + 4\pi \alpha M(H)] \sin\theta. \quad (6)$$

Note that in this approach, the parameter α is simply a numerical coefficient independent of the external field direction. However, orientational dependences of the effective field (6) and, consequently, the magnetoresistance hysteresis originate from the fact that the projections of $\boldsymbol{B}_{ind}$ and $\boldsymbol{H}$ onto the $\boldsymbol{s}$ axis change with angle θ. The effective field determined from (6) affects the dissipation processes in the intergrain boundaries.

Certainly, Eq. (6) only works for the ideal ordered systems consisting of grains with the same shape and size separated by the identical intergrain spacings. In real granular systems, we cannot expect that the conditions $\boldsymbol{n} \parallel \boldsymbol{B}_{ind}$ and $\boldsymbol{n} \parallel \boldsymbol{H}$ for $\theta = 0$ and $\boldsymbol{n} \perp \boldsymbol{B}_{ind}$ and $\boldsymbol{n} \perp \boldsymbol{H}$ for $\theta = \pi/2$ will be strictly satisfied due to the presence of microscopic trajectories of current $\boldsymbol{I}$, which are nonparallel to macroscopic current $\boldsymbol{j}$. It is well-known[7-12,18-21,27-30] that even at $\theta = 0$ the magnetoresistance of granular HTS samples is nonzero and exhibits the hysteresis. Previously, the α value (~10) for $\theta = 0$ [27-29] was estimated. In view of the aforesaid, we may assume that for real granular superconductors Eq. (6) can be rewritten with regard to the isotropic (independent of θ) contribution:

$$B_{eff,s}(H) = H(C_{is} + C_{anis} \sin\theta) + 4\pi M(H)(\alpha_{is} + \alpha_{anis} \sin\theta). \quad (7)$$

Here, the introduced constants C_{is}, C_{anis}, α_{is}, and α_{anis} correspond to the isotropic and anisotropic effects of the field and magnetic moments of grains. There is the obvious correlation between $C_{is} + C_{anis} = 1$ and $\alpha_{is} + \alpha_{anis} = \alpha$, where α is determined from Eq. (3) and enters Eq. (6) as an orientation-independent parameter. We assume the isotropic parameters C_{is} and α_{is} to be caused by the fact that real granular systems differ from the ideal model. In addition, according to our data and the results reported in Ref. 41 for non-textured granular HTSs, the magnetic moment weakly depends on the mutual direction of the external field and orientation of the sample sides (the difference between the magnetic moments at $\boldsymbol{H} \parallel \boldsymbol{L}$ and $\boldsymbol{H} \perp \boldsymbol{L}$ is only a few percent). Consequently, orientational dependence (7) is expected to remain proportional to $\sin\theta$. Below, based on the experimental data, we demonstrate that, indeed, the dependence similar to (7) is observed.

4. Results and discussion

Figure 4 shows the $R(H)$ dependences for the YBCO sample obtained at T = 77.4 K and different angles $\theta = \angle \boldsymbol{H}, \boldsymbol{j}$ with a step of 10^0. A part of the $R(H)$ dependence starting with the origin of coordinates corresponds to the initial path after ZFC. In these experiments, after recording of the total loop in fields of up to ± 500 Oe, the external-field direction was sequentially changed. One can clearly see the anisotropy of the hysteretic properties of magnetoresistance.

Figure 5 presents enlarged portions of the $R(H)$ hysteretic dependences. The dashed horizontal lines give an example of determination of the magnetoresistance hysteresis width $\Delta H = H_{dec} - H_{inc}$ at $H_{dec} = 450$ Oe. It can be seen that the ΔH value decreases with the angle θ (the ΔH value is maximum at $\theta = 90^0$ and minimum at $\theta = 0^0$).

To further analyze the parameter ΔH, we use the experimental $M(H)$ hysteresis data. Figure 6 shows the $M(H)$ dependence measured on the sample for which the data from Figs. 4 and 5 were obtained. As is known, in granular HTSs the hysteresis loop asymmetry relative to the abscissa axis increases with temperature[41-46]. In other words, at low temperatures we have $|M(H_\uparrow)| \approx |M(H_\downarrow)|$ at $H_\uparrow = H_\downarrow$ (Fig. 1a), while at high temperatures the inequality $|M(H_\uparrow)| > |M(H_\downarrow)|$ is valid. In addition, the $M(H_\downarrow)$ values remain negative in a wide magnetic field range (Fig. 6). This asymmetry of the hysteresis loops is caused by the contribution of the equilibrium (hysteresisless) magnetization of the grain surface layer [42, 44]. At low temperatures, the relative contribution of surface magnetization is smaller than the contribution of nonequilibrium magnetization of the bulk of the sample. At high temperatures, the grain surface region size increases and, consequently, the equilibrium magnetization fraction in the total magnetization loop grows[44]. However, for the above-described modification of the $M(H)$ dependences, the field distribution in the intergrain medium (Fig. 1a) will remain nearly invariable, since even at $M(H_\downarrow) < 0$ the inequality $B_{eff}(H = H_\uparrow) > B_{eff}(H = H_\downarrow)$ is still valid due to the condition $|M(H_\uparrow)| > |M(H_\downarrow)|$ and the $R(H)$ hysteresis is obvious.

Estimation of the intragrain critical current from the data presented in Fig. 6 using the Bean formula $J_{CG}(A/cm^2) \sim 30\, \Delta M(emu/cm^3)/2R(cm)$ yields (at $R \sim 3$ μm) $J_{CG} \sim 1.5 \div 2 \cdot 10^5$ A/cm^2 in fields of up to 100 Oe. This value exceeds the critical transport current $J_C(H = 0) \approx 10^2$ A/cm^2 by a few orders of magnitude,

which confirms the model assumption about the occurrence of dissipation only in the intergrain spacings (inequality $J_{Cgrain}(H) >> J_{C\ intergrain}(H)$, see Sec. 3.1).

Figure 7 shows the absolute value of the effective field in the intergrain medium $|B_{eff}(H)|$ as a function of the external field. The $|B_{eff}(H)|$ dependences were built using Eq. (4) on the basis of experimental data presented in Fig. 6. Hereinafter, we omit indices z and s for the experimental effective fields. In addition, the absolute value of Eq. (4) was taken, since the field sign is unimportant for the magnetoresistance: $R \sim |B_{eff}(H)|$. In (4), parameter α is simply a numerical coefficient independent of the field direction, but, according to dependences (5) and (6), there is the field–current orientational dependence. When building the $|B_{eff}(H)|$ dependences on the basis of Eq. (4) at different orientations $\theta = \angle \boldsymbol{H}, \boldsymbol{j}$ (Fig. 7), we used the only fitting parameter, specifically, the effective value $\alpha = \alpha_{eff}$ depending on angle θ. Comparing with Eq. (7), obtain

$$\alpha_{eff} = \alpha_{is} + \alpha_{anis} \sin\theta. \quad (8)$$

A criterion for building the $|B_{eff}(H)|$ dependences and obtaining the α_{eff} value was the best agreement between the hysteresis loop width $\Delta H = H_{\downarrow} - H_{\uparrow}$ at $B_{eff}(H_{\downarrow}) = B_{eff}(H_{\uparrow})$ and that for the $R(H)$ dependences (Figs. 4 and 5) in the wide field range. The α_{eff} values are presented in Fig. 7. Horizontal dashed lines in Fig. 7 show the example of determination of the hysteresis width $\Delta H = H_{dec} - H_{inc}$ at $H_{inc} = 450$ Oe for the $B_{eff}(H)$ dependences.

A comparison of the $R(H)$ hysteretic dependences in Figs. 4 and 5 and $|B_{eff}(H)|$ (Fig. 7) allows us to speak about their satisfactory agreement, taking into account that the magnetoresistance is determined by the expression similar to (1): $R \sim \exp(-U_P(|B_{eff}(H)|, T, j) / k_B T)$. The minimum in the $R(H_{dec})$ and $|B_{eff}(H_{dec})|$ dependences is observed at the maximum compensation of the external field and the field $\boldsymbol{B}_{ind}$ induced by the magnetic moments of grains.

Figure 8 shows the dependences of the ΔH value on the field H_{dec} obtained from the experimental $R(H)$ hysteretic dependences (Figs. 4 and 5) at several angles θ and the $|B_{eff}(H)|$ dependences (Fig. 7) calculated at different α_{eff} values presented in the figure. The satisfactory agreement between the experimental and calculated ΔH values is observed, at least, in fields above 200 Oe[47]. The inset in Fig. 7 presents the ΔH values at $H_{dec} = 450$ Oe as a function of angle θ for the $R(H)$ and $|B_{eff}(H)|$ dependences, i.e., in fact, the lengths of horizontal segments in Figs. 5 and 7.

Figure 9 shows the parameter α_{eff} obtained at the best agreement between the field hysteresis loop $\Delta H(H_{dec})$ obtained from the $R(H)$ and $|B_{eff}(H)|$ data (Fig. 8) as a function of angle θ. The solid line in Fig. 9 was built using dependence (8) at $\alpha_{is} = 10$ and $\alpha_{anis} = 12.5$; i.e., sinusoidal dependence (6) proposed by Daghero et al. (Ref. 12) really exists. The similarity between the α_{is} and α_{anis} values indicates that in the systems of the granular HTS type, some trajectories of microscopic currents $\boldsymbol{I}$ have the direction different from the direction of macroscopic current $\boldsymbol{j}$ (see Sec. 3.3). In the idealized picture in Fig. 3a, the effect of both external $\boldsymbol{H}$ and induced $\boldsymbol{B}_{ind}$ field, as well as the effect of flux compression on carrier tunneling should be negligible, since the components $B_{ind,z} \sin\theta$ and $H \sin\theta$ are zero. However, it was found that the induced field and, consequently, the flux compression significantly affect also carrier tunneling at the parallel configuration $\boldsymbol{H} \parallel \boldsymbol{j}$. On the other hand, the validity of functional dependence (6) can be a confirmation of the approach used to describe the magnetotransport properties of granular HTSs.

5. Summary

The angular (magnetic field–transport current direction) dependence of magnetoresistance hysteresis in the granular yttrium HTSs was measured and analyzed. Based on the model representations from Ref. 12 and the developed approach to the analysis of magnetoresistance hysteresis[27–29], we investigated the effect of magnetic flux compression in the intergrain medium on carrier tunneling at different mutual orientations of the macroscopic current $\boldsymbol{j}$ and external field $\boldsymbol{H}$. Using the proposed model, we established and experimentally confirmed that the magnetoresistance is determined by the effective field component $\boldsymbol{B}_{eff}$ (relative to the flux compression) perpendicular to the macroscopic current direction, i.e., in fact, $R \sim B_{eff,z} \sin(\boldsymbol{H}, \boldsymbol{j})$. Meanwhile, the orientational dependence of magnetoresistance, as well as the R(H) hysteresis parameter, contains also the term independent of the angle $\theta = \angle \boldsymbol{H}, \boldsymbol{j}$, i.e., isotropic relative to the $\boldsymbol{H}$ and $\boldsymbol{j}$ orientations. This can be caused by the deviation of grain morphology in real crystals from the model representation of grains with the same shape and size.

The significant magnetic flux compression is reflected in both the parallel ($\boldsymbol{H} \parallel \boldsymbol{j}$) and perpendicular ($\boldsymbol{H} \perp \boldsymbol{j}$) configurations. The parameter α characterizing the degree of magnetic flux compression in the intergrain medium is ~20 and the maximum effect on the magnetoresistance is observed at the orientation

$\boldsymbol{H} \perp \boldsymbol{j}$. At $\boldsymbol{H} \parallel \boldsymbol{j}$, the effect of magnetic flux compression is almost twofold weaker and the orientational portion follows the dependence proportional to $\sin(\boldsymbol{H}, \boldsymbol{j})$.

It is the flux compression that determines the fairly wide magnetoresistance (and the critical current) hysteresis in granular HTSs in the field range where the external field H is much weaker than the field induced by grains ($4\pi \alpha M(H)$). In the yttrium HTS, this external field range is from ~ 10^2 to ~ 10^3 Oe at liquid nitrogen temperatures. With a further increase in the external field (or at approaching the transition temperature T_C), the effect of magnetic moments of grains on the intergrain medium weakens and the $R(\boldsymbol{H} \parallel \boldsymbol{j})/R(\boldsymbol{H} \perp \boldsymbol{j})$ value tends to unity, which is consistent with the model representations from Ref. 12.

In the authors' opinion, the above consideration is applicable to, at least, non-textured YBCO, LSCO, and BSCCO granular HTSs in the magnetic field and temperature ranges where the dissipation only occurs in the grain boundary subsystem. The description of the transition of the HTS grain subsystem to the ground state under the action of magnetic field (or temperature) needs in other mechanisms of the HTS grain anisotropy effects[46].

Acknowledgments

We are grateful to M. Petrov for preparation of the sample, A. Krasikov for help, and D. Gokhfeld, A. Dubrovskiy, and D. Velikanov for useful discussions.

This study was supported by the Russian Foundation for Basic Research, Government of the Krasnoyarsk Territory, and Krasnoyarsk Territorial Foundation for Support of Scientific and R&D Activities, research project no. 16-48-243018.

References

1Y. Yeshurn, A.P. Malozemoff, A. Shaulov, Rev. Mod. Phys., **68**, 911 (1993).

2L. Ji, M.S. Rzchowski, N. Anand, and M. Tinkham., Phys. Rev B **47**, 470 (1993).

3J. Ayache, Philosophical Magazine **86**, 2193 (2006)

4L. Bulaevskii, J.R. Clem, L.I. Glazman, A.P. Malozemoff, Phys. Rev. **B 45**, 2545 (1992).

5B. Hensel, J.-C. Grivel, A. Jeremie, A. Perin, A. Pollili, R. Flükiger, Physica **C 205**, 329 (1993).

6B. Hensel, G. Grasso, R. Flükiger, Phys. Rev. **B 51**, 15456 (1995).

7D. Lopez, F. De la Cruz, *Phys. Rev. B* **43** 11478 (1991)

8D. López, R. Decca, F. De la Cruz, *Solid State Commun.* **79** 959-962 (1991)

9D. López, R. Decca, F. De la Cruz, *Supercond. Sci. Technol.* **5** 276 (1992)

10M.M. Asim, S.K. Hasanain, *Solid State Commun.* **80** 719-723 (1991)

11A. Kiliç, K. Kiliç, S. Senoussi and K. Demir, *Phys.* C **294** 203-216 (1998)

12D. Daghero, P. Mazzetti, A. Stepanescu, P. Tura, A. Masoero, *Phys. Rev.* B **66** 184514 (2002)

13Y.J. Quian, Z.M. Tang, K.Y. Chen, B. Zhou, J.W. Qui, B.C. Miao, Y.M. Cai, Phys. Rev. B **39**, 4701 (1989).

14J. E. Evetts and B. A. Glowacki, Cryogenics **28**, 641 (1988).

15M.N. Kunchur, T.R. Askew, J. Appl. Phys. **84** (N12), 6763 (1998).

16N.D. Kuz'michev, JETP Lett. **74** (5), 262 (2001).

17P. Mune, F.C. Fonseca, R. Muccillo, R.F. Jardim, Physica C, **390**, 363 (2003).

18T.V. Sukhareva, V.A. Finkel, Phys. Solid State **50** 1001 (2008).

19T.V. Sukhareva and V.A. Finkel', JETP 107, 787 (2008).

20V.V. Derevyanko, T. V. Sukhareva, and V. A. Finkel, Technical Physics **53**, 321 (2008).

21M. Olutas, A. Kilic, K. Kilic, and A. Altinkok, Eur. Phys. J. B, **85**, 382 (2012).

22M. Olutas, A. Kilic, K. Kilic, A. Altinkok, J. Supercond. Nov. Magn. **26**, 3369 (2013).

23A. Altinkok, K. Kilic, M. Olutas, A. Kilic, J. Supercond. Nov. Magn. **26**, 3085 (2013).

24D.A. Balaev, A.A. Dubrovskii, S.I. Popkov, K.A. Shaykhutdinov, M.I. Petrov, Physics of the Solid State, **50**(6) 1014 (2008).

25D.A. Balaev, D.M. Gokhfeld, A.A. Dubrovskii, S.I. Popkov, K.A. Shaykhutdinov, M.I. Petrov, JETP **105**, 1174 (2007).

26D.A. Balaev, A.A. Dubrovskii, K.A. Shaykhutdinov, S.I. Popkov, D.M. Gokhfeld, Yu.S. Gokhfeld, M.I. Petrov, JETP **108**, 241 (2009).

27D.A. Balaev, S.I. Popkov, E.I. Sabitova, S.V. Semenov, K.A. Shaykhutdinov, A.V. Shabanov, M.I. Petrov, J. Appl. Phys. **110**, 093918 (2011).

28D.A. Balaev, S.V. Semenov, and M.I. Petrov, Physics of the Solid State **55** (12), 2422 (2013).

29D.A. Balaev, S.V. Semenov, M.I. Petrov, J. Supercond. Nov. Magn. **27**, 1425 (2014).

30D.A. Balaev, A.G. Prus, K.A. Shaukhutdinov, D.M. Gokhfeld, M.I. Petrov, Supercond. Sci. Technol. **20**, 495 (2007).

31D.A. Balaev, A.A. Bykov, S.V. Semenov, S.I. Popkov, A.A. Dubrovskii, K.A. Shaykhutdinov, M.I. Petrov, Physics of the Solid State, **53**(5) 922 (2011).

32D.A. Balaev, S.I. Popkov, S.V. Semenov, A.A. Bykov, E.I. Sabitova, A.A. Dubrovskiy, K.A. Shaikhutdinov, M.I. Petrov, J Supercond Nov Magn **24**, 2129 (2011).

33C.P. Bean. Rev. Mod. Phys. **36**, 31 (1964).

34V. V. Val'kov and B. P. Khrustalev, J. Exp. Theor. Phys. **80** (4), 680 (1995).

35J.Jung M. A.-K. Mohamed, S. C. Cheng, and J. P. Franck, Phys. Rev. B **42**, 6181 (1990)

36B. Andrzejewski, E. Guilmeau, Ch. Simon, .Supercond. Sci. Technol. **14**, 904 (2001).

37D.A. Balaev, A.A. Dubrovskii, S.I. Popkov, D.M. Gokhfeld, S.V. Semenov, K.A. Shaykhutdinov, M.I. Petrov, Physics of the Solid State, **54**(11) 2155 (2012).

38J. Barden, M.J. Stephen, Phys. Rev. **140** (N 4A), A1197 (1965).

39W.K. Kwok, U. Welp, G.W. Crabtree, K.G. Vandervoot, R. Hulscher and J.Z. Liu, Phys. Rev. Lett. **64** (8), 966 (1990).

40The parameter k introduced in [12] is the coefficient of external field compression in the intergrain spacings. In comparison with Eq. (4) ($B_{\text{eff},z} = k\,H$), it is related to the parameter α used by us as $k = 1 + 4\pi\,\alpha\,(M/H)$.

41V.V. Makarov, Phys. Solid State **35**, 22 (1993).

42D.-X. Chen, R.B. Goldfarb, R.W. Cross, A. Sanchez. Phys. Rev.B **48**, 6426 (1993)

43D.M. Gokhfeld, D.A. Balaev, M.I. Petrov, S.I. Popkov, K.A. Shaykhutdinov, and V.V. Val'kov, J. Appl. Phys. **109**, 033904 (2011).

44D.M. Gokhfeld, Phys. Solid State **56**, 2380 (2014).

45I.A. Golovchanskiy, A.V Pan, J. George, F.S. Wells, S.A. Fedoseev, A. Rozenfeld, Supercond. Sci. Technol. **29**, 075002 (2016).

46M. Eisterer, M. Zehetmayer, and H.W.Weber, Phys. Rev. Lett. **90**, 247002 (2003).

47A certain deviation from the fits in Fig. 8 in weak magnetic fields originates from the fact that relation (3) is not quite applicable in the vicinity of "zero magnetization" ($M \approx 0$). Indeed, the "zero magnetization" results from the equality of magnetic contributions of the screening (Meissner) currents (on the grain surface) and Abrikosov vortices (within grains). These contributions, however, can lead to the nonzero magnetic induction in the spacings between neighboring grains.

Figure captions

Figure 1. Hysteretic field dependences of (**a**) magnetization $M(H)$ and (**b**) magnetoresistance $R(H)$ for the YBCO *composite* sample at $T = 4.2$ K. (**a**) Schematic of the lines of magnetic induction $\boldsymbol{B}_{ind}$ in the intergrain medium induced by magnetic moments $\boldsymbol{M}_G$ of superconducting grains (ovals) at the increasing field $\boldsymbol{H} = \boldsymbol{H}_{inc}$ (in the bottom, $M(H_{inc}) < 0$) and decreasing field $\boldsymbol{H} = \boldsymbol{H}_{dec}$ (on the top, $M(H_{dec}) > 0$). In this schematic representation, the axes $\boldsymbol{z}$ is parallel to $\boldsymbol{H}$ and directed upwards. In (**b**), an example of determination of the hysteresis field width $\Delta H = H_{dec} - H_{inc}$ is shown; in (**a**), the $M(H_{inc})$ and $M(H_{dec})$ values corresponding to the magnetic state of the sample are marked. Arrows indicate the direction of variation in external field H.

Figure 2. Schematic of the magnetic induction lines in the intergrain medium from magnetic moments $\boldsymbol{M}_G$ of superconducting grains. (**a**) Grains (ovals) are far from each other. (b) Crowding of magnetic induction lines at the small intergrain spacing (flux compression); the dashed line (red) shows the trajectory of microscopic current $\boldsymbol{I}$ for the perpendicular configuration $\boldsymbol{H} \perp \boldsymbol{j}$. The external field $\boldsymbol{H} = \boldsymbol{H}_{inc}$ increases in both (**a**) and (**b**). Note that the intergrain distance in (a) and (b) is enlarged: in real granular HTSs, the grain boundary length is much smaller than the grain size (see Section *3.2* for more detail).

Figure 3. Schematic of the magnetic induction lines and trajectories of microscopic current $\boldsymbol{I}$ (dashed lines) for (**a**) the parallel ($\boldsymbol{H} \parallel \boldsymbol{j}$) and (**b**) perpendicular ($\boldsymbol{H} \perp \boldsymbol{j}$) configurations and (**c**) at a certain intermediate angle $\theta = \angle \boldsymbol{H}, \boldsymbol{j}$. To explain the model representations, the axes $\boldsymbol{z}$ (parallel to $\boldsymbol{H}$ and directed upwards), $\boldsymbol{n}$ (normal to the intergrain boundary plane S), and $\boldsymbol{s}$ (perpendicular to $\boldsymbol{n}$ and lying in the plane formed by the vectors $\boldsymbol{H}$ and $\boldsymbol{I}$) are introduced. The spacings between neighboring grains are significantly enlarged.

Figure 4. Hysteretic field dependences of magnetoresistance $R(H)$ for the YBCO sample at $T = 77.4$ K and different $\boldsymbol{H}$ and $\boldsymbol{j}$ orientations ($\theta = \angle \boldsymbol{H}, \boldsymbol{j}$). Arrows indicate the direction of variation in external field H.

Figure 5. Enlarged positive-field portion from Fig. 4. Horizontal dashed lines correspond to the hysteresis field width ΔH at $H_{dec} = 450$ Oe and different angles $\theta = \angle \boldsymbol{H}, \boldsymbol{j}$.

Figure 6. Magnetic hysteresis of the YBCO sample at $T = 77.4$ K. Arrows indicate the direction of variation in external field H.

Figure 7. Hysteretic dependences of the effective field $|B_{eff}(H)|$ in the intergrain medium obtained from Eq. (4) using the $M(H)$ data from Fig. 6 and parameters α_{eff} shown in the figure. Horizontal dashed lines correspond to the hysteresis field width ΔH at $H_{dec} = 450$ Oe and different angles $\theta = \angle \boldsymbol{H}, \boldsymbol{j}$. Arrows indicate the direction of variation in external field H.

Figure 8. Dependence of the hysteresis field width ΔH on H_{dec} obtained using the $R(H)$ data from Figs. 4 and 5 (symbols) and $|B_{eff}(H)|$ (Fig.7) at the indicated α_{eff} values. Inset: ΔH vs angle $\theta = \angle \boldsymbol{H}, \boldsymbol{j}$ at $H_{dec} = 450$ Oe (these data correspond to the lengths of horizontal segments in Figs. 5 and 7).

Figure 9. Orientational dependence of parameter α_{eff} (Eqs. (3) and (4)) obtained from the condition for the consistency of the $\Delta H(H_{dec})$ data in Fig. 8 (symbols). The solid line is built using Eq. (8).

This manuscript was accepted by J. Appl. Phys. Click here to see the version of record.

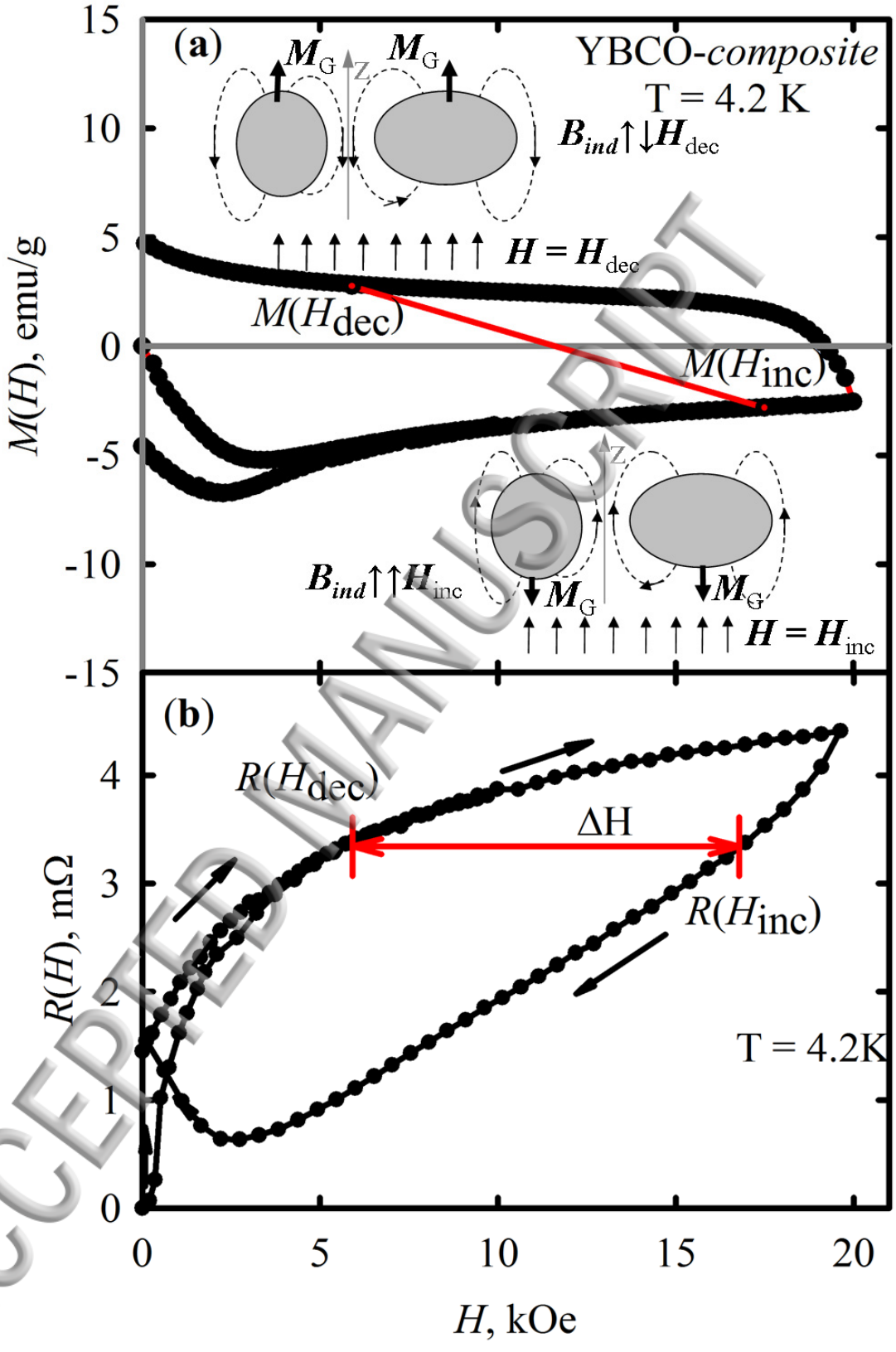

Figure 1.

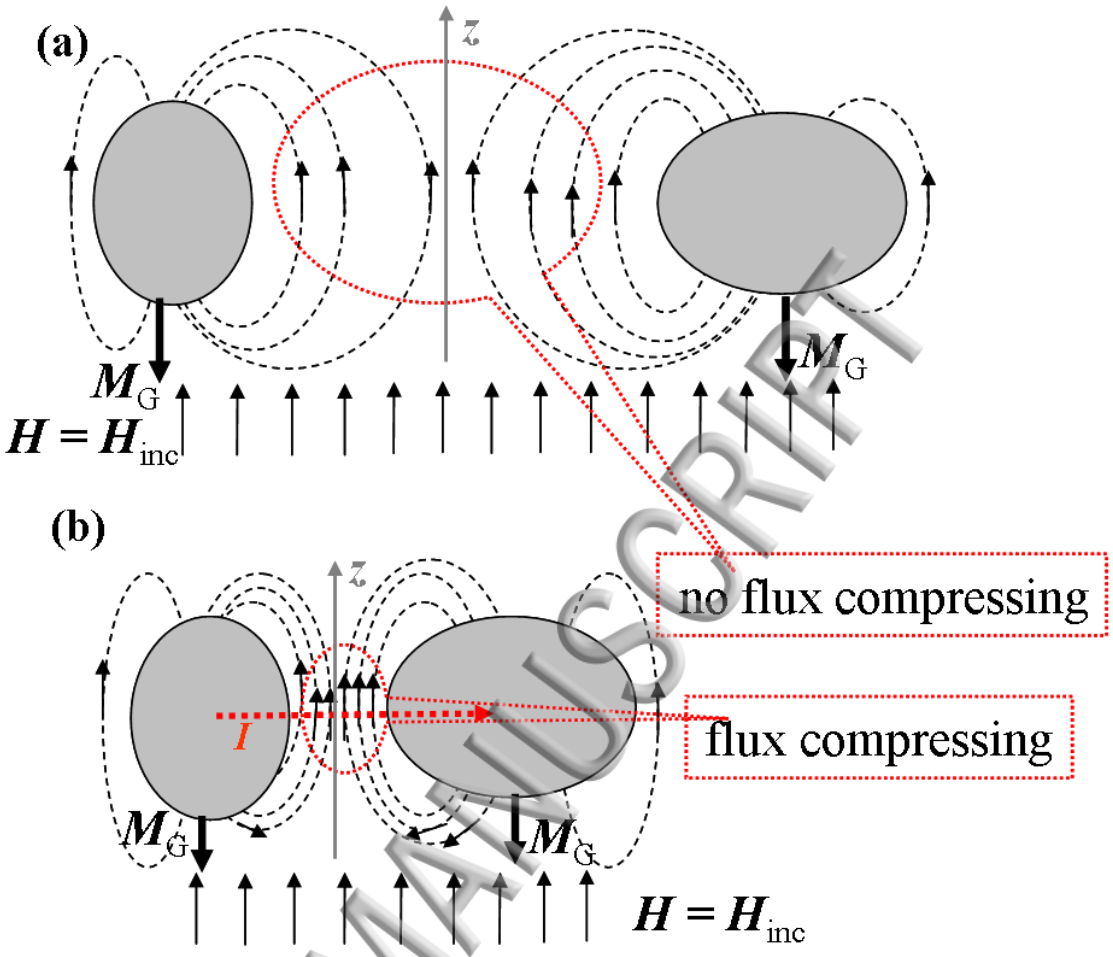

Figure 2.

This manuscript was accepted by J. Appl. Phys. Click here to see the version of record.

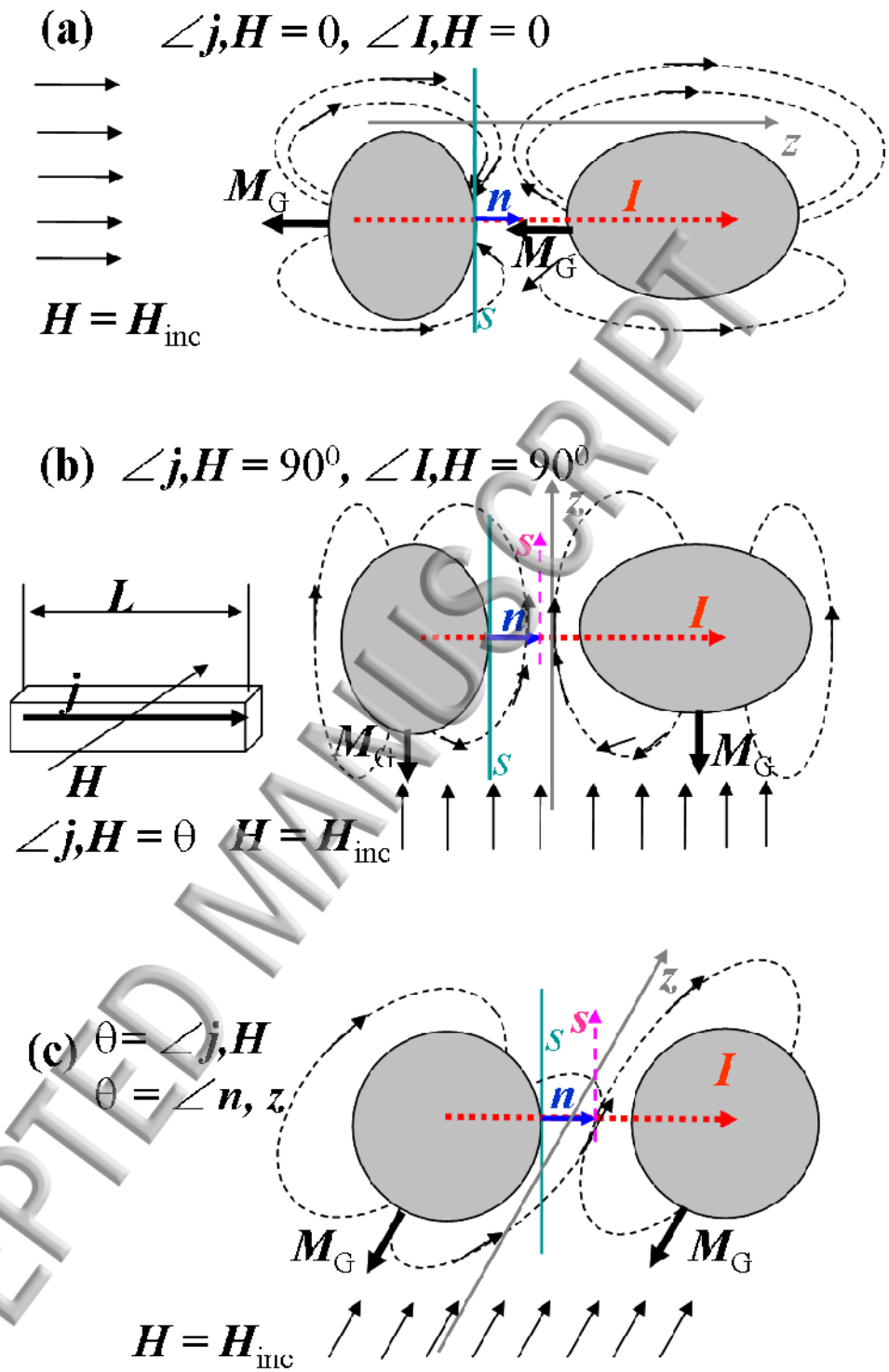

Figure 3.

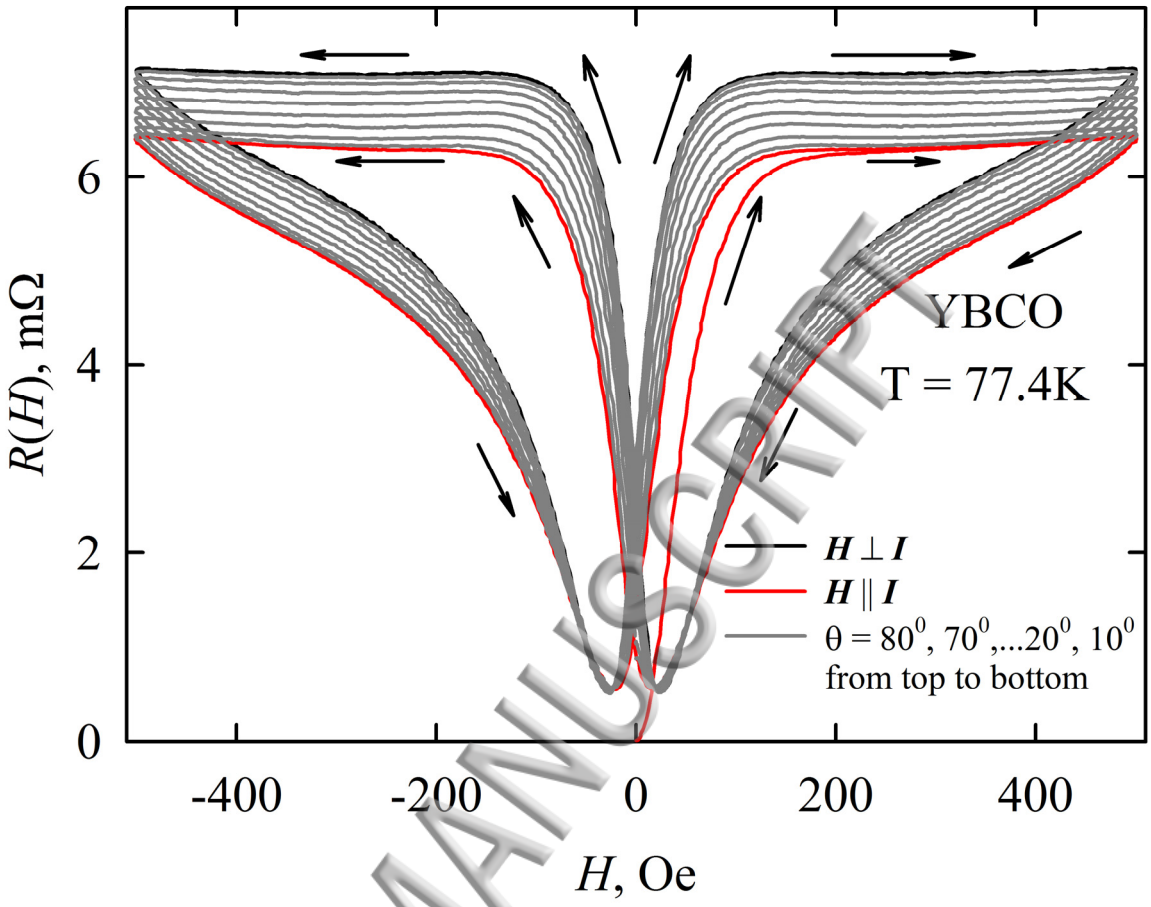

Figure 4.

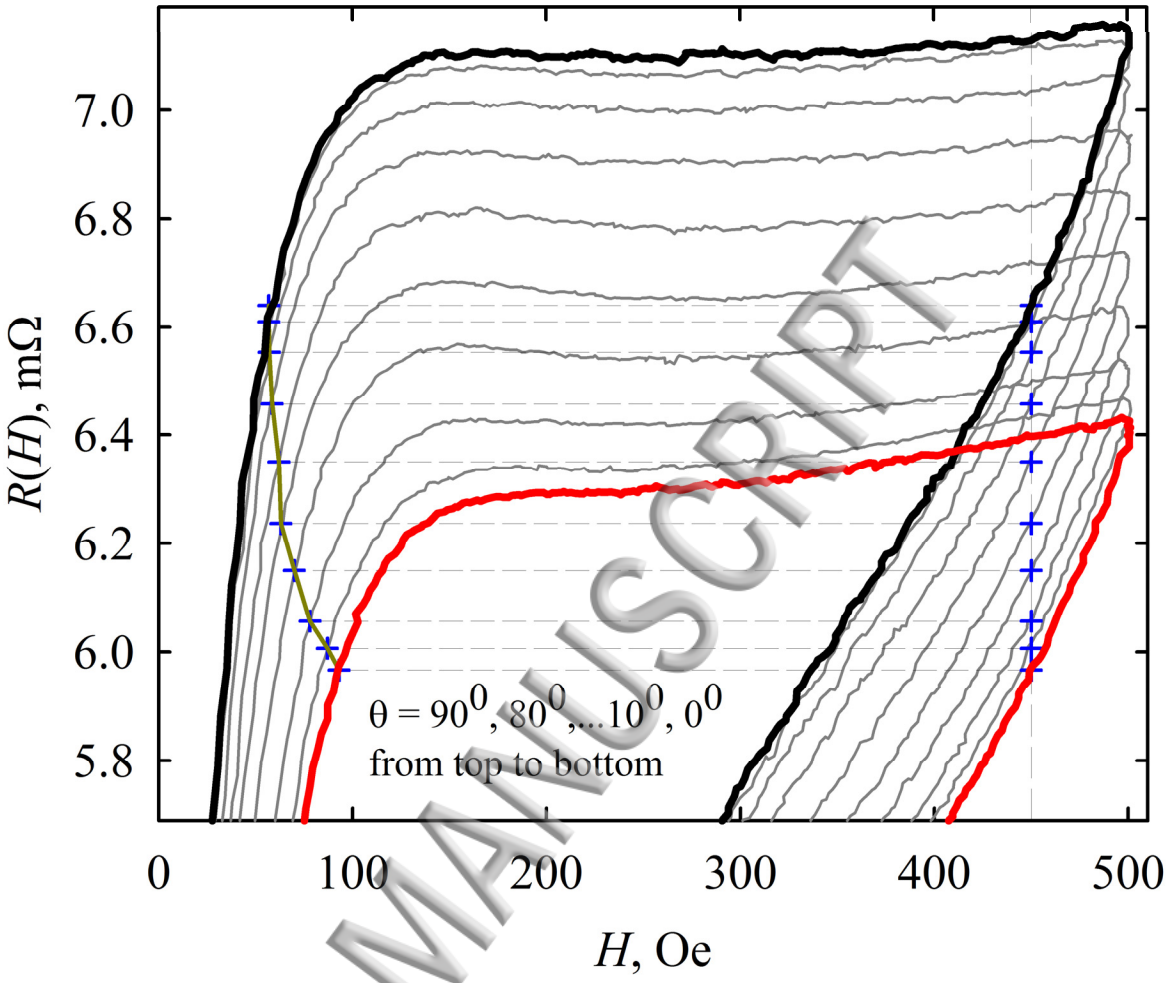

Figure 5.

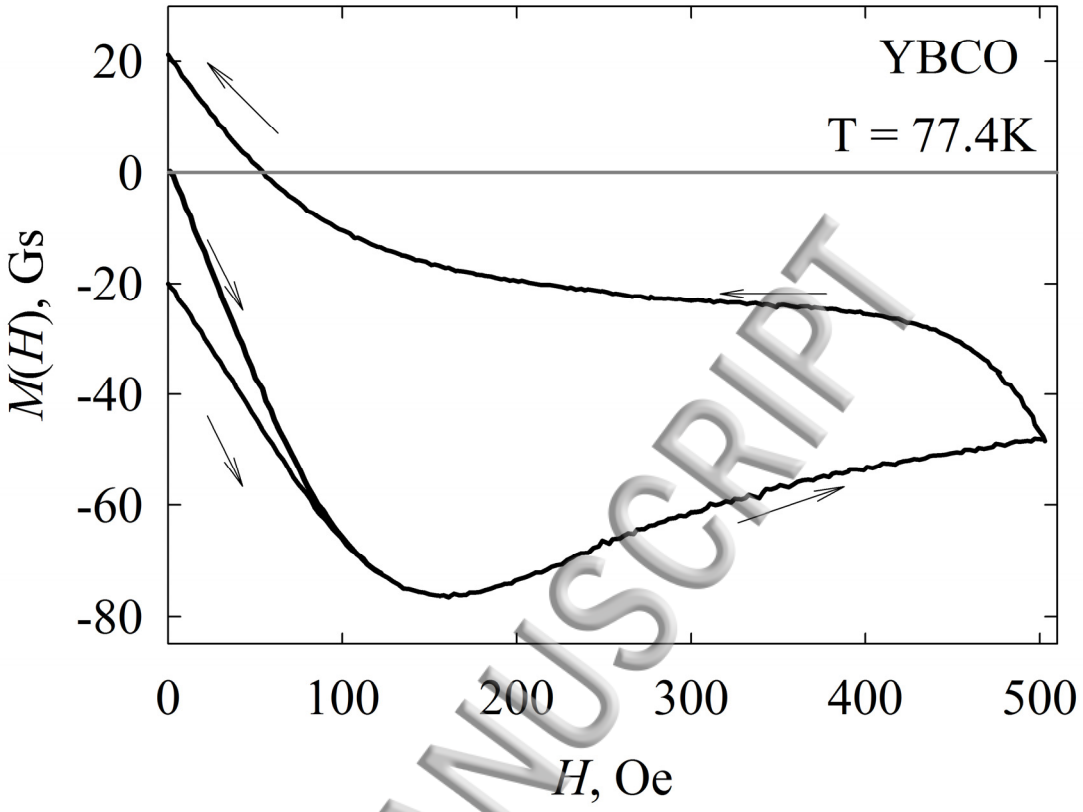

Figure 6.

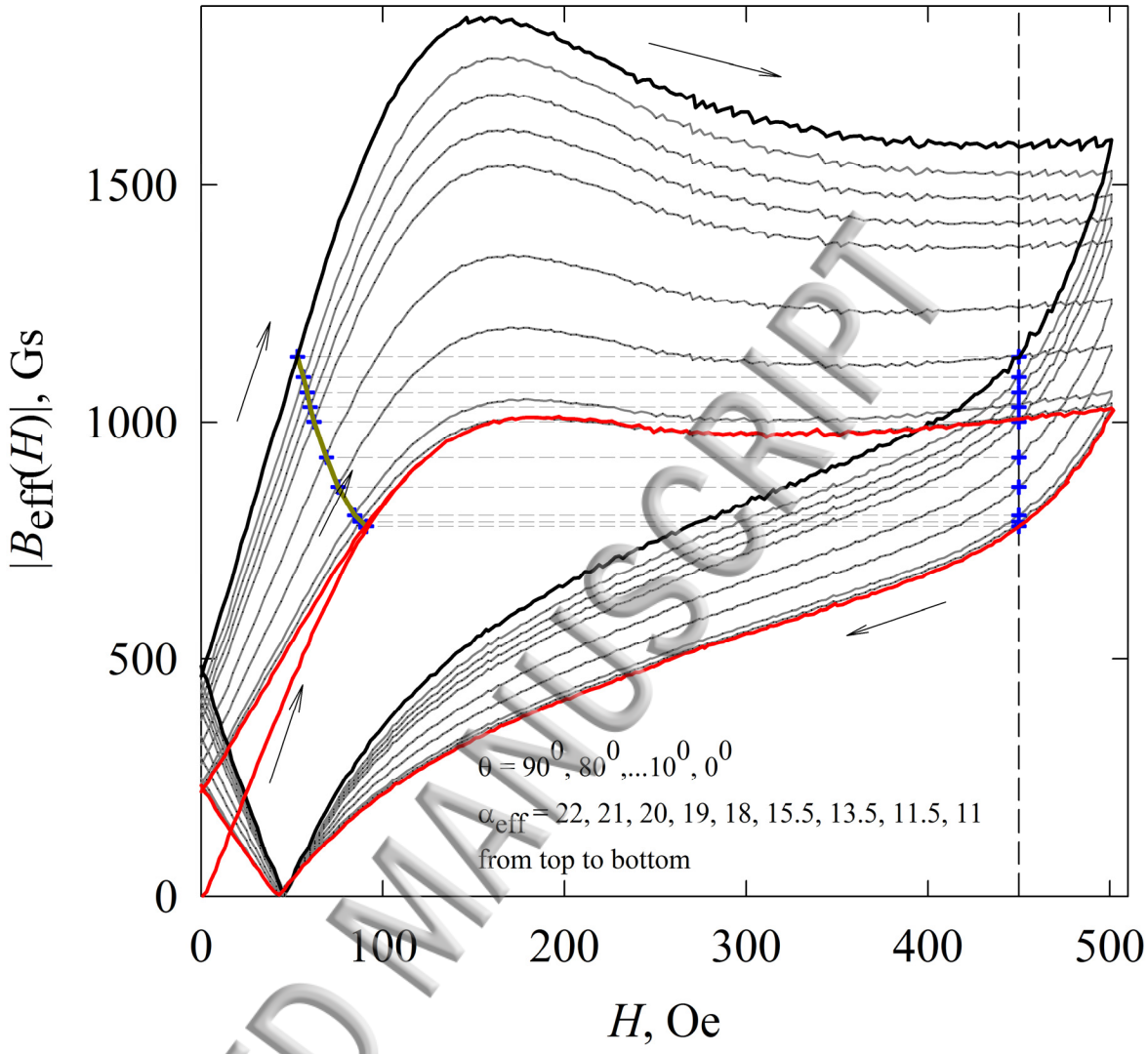

Figure 7.

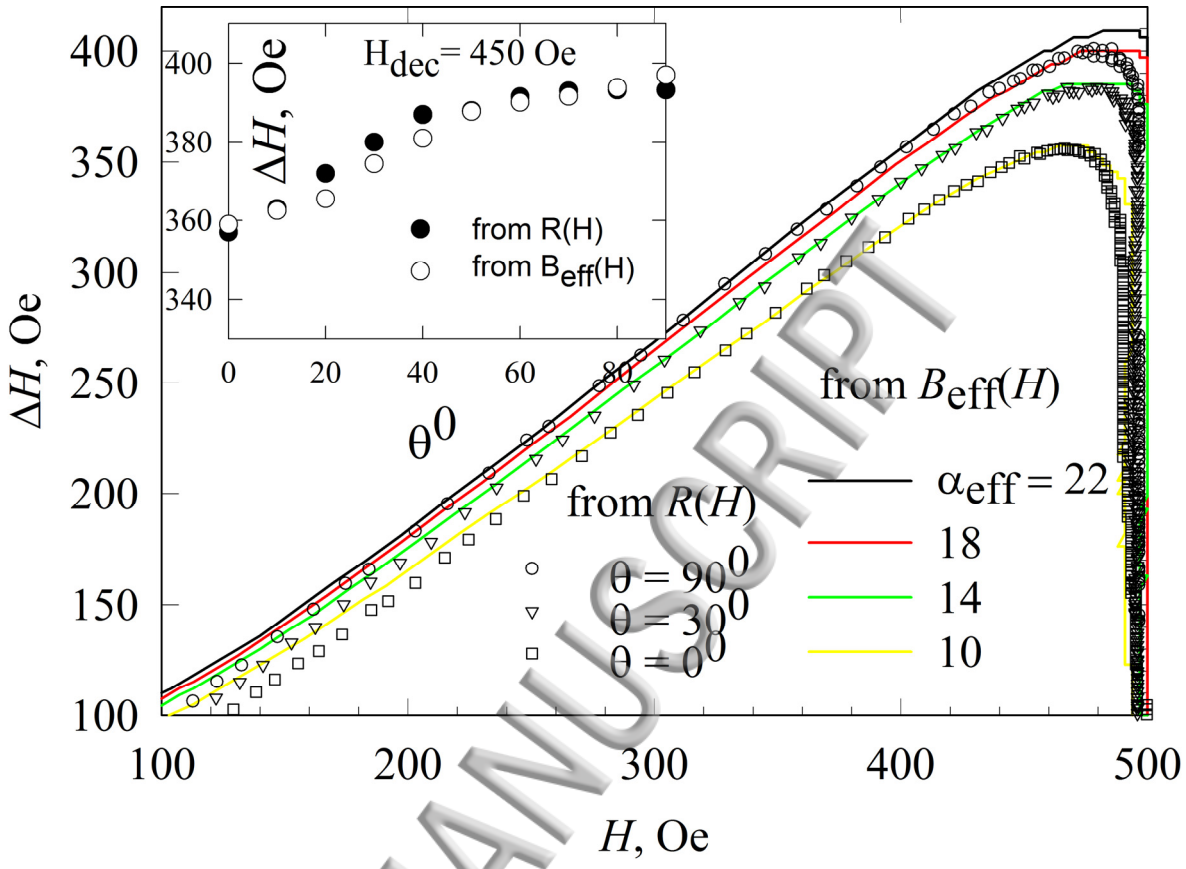

Figure 8.

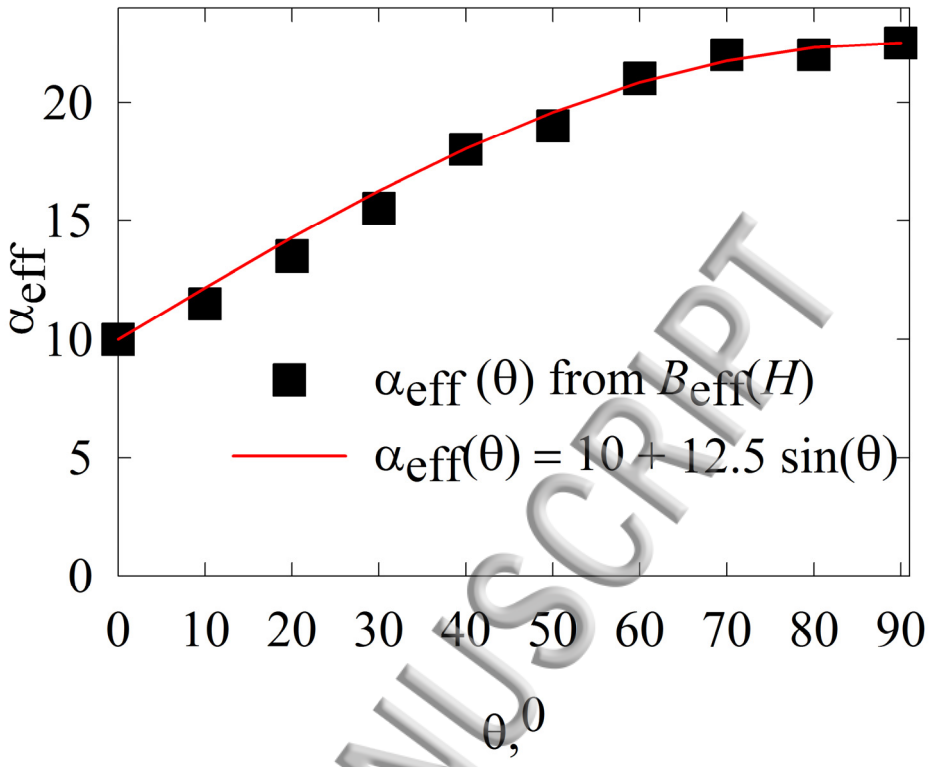

Figure 9.

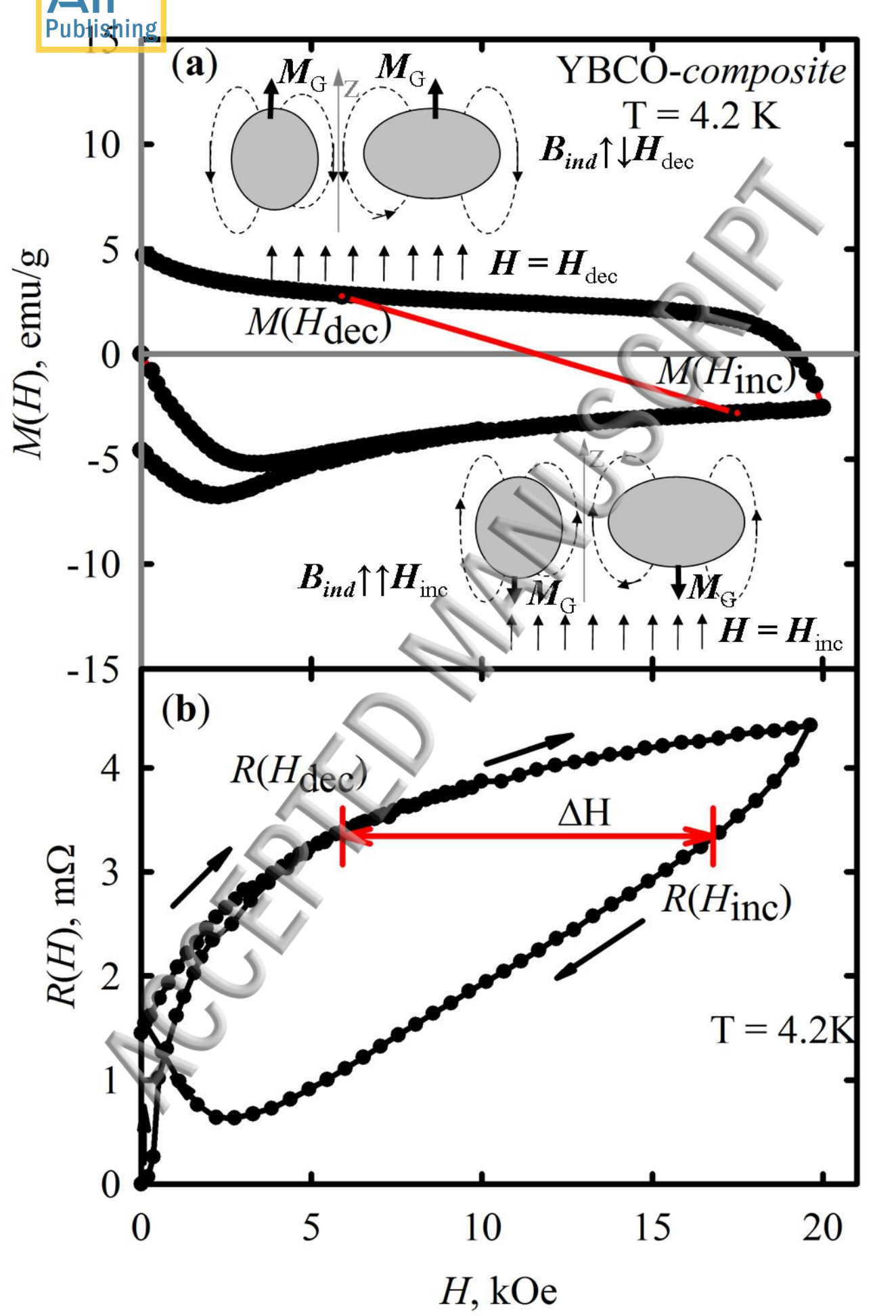

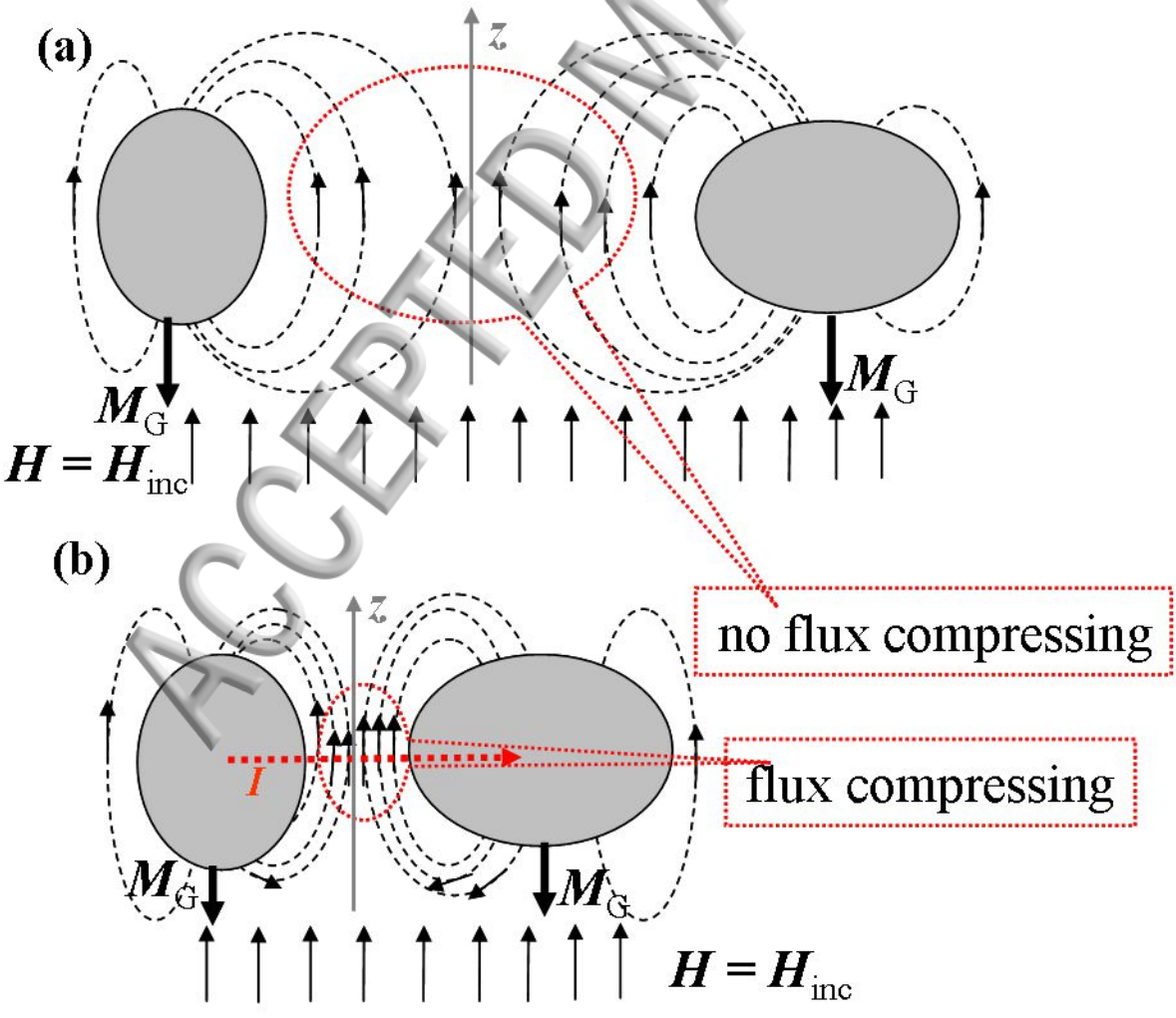
(a)
z
M_G
M_G
$H = H_{inc}$
(b)
z
no flux compressing
flux compressing
I
M_G
M_G
$H = H_{inc}$

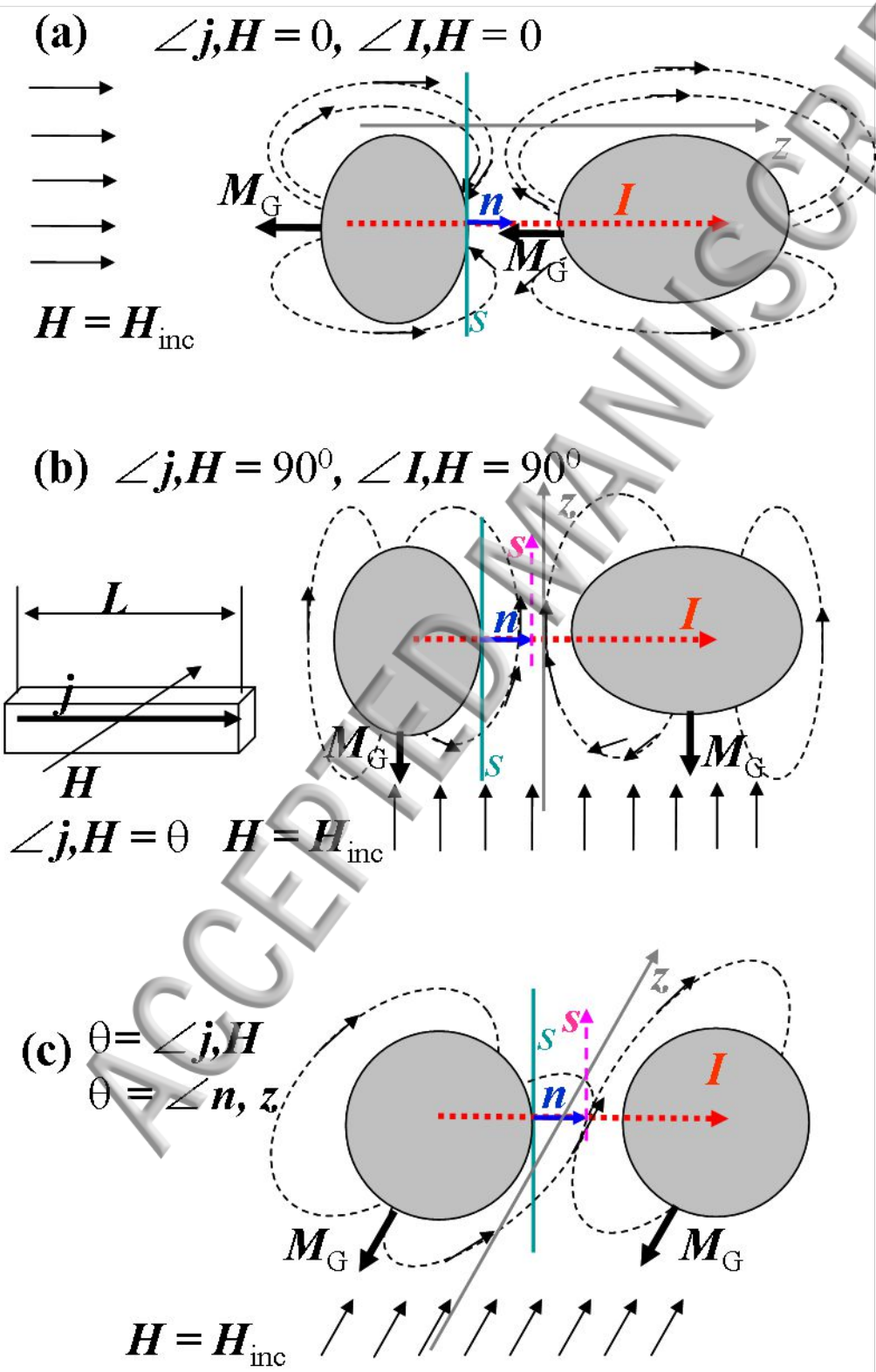

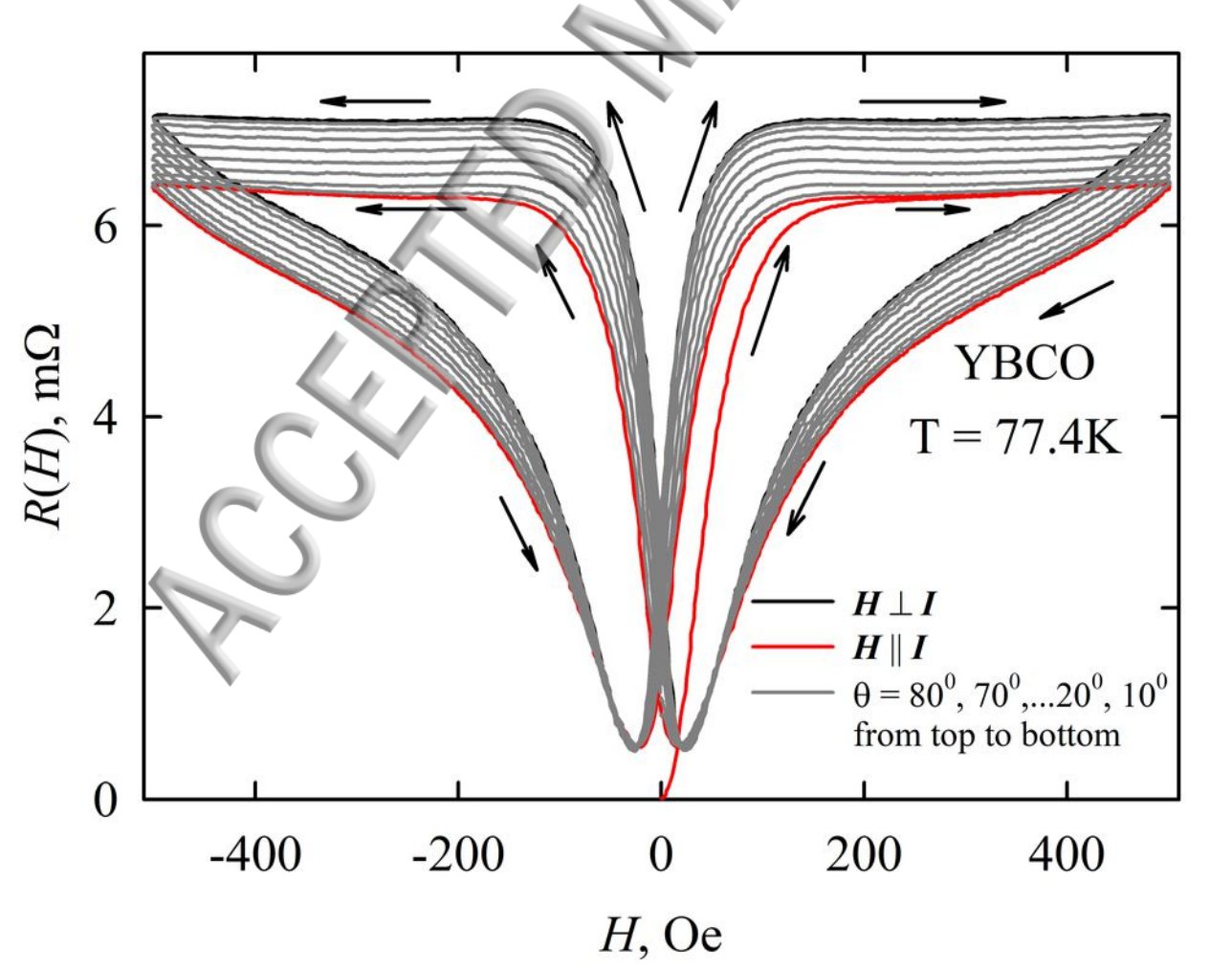
R(H), mΩ
6
4
2
0
-400
-200
0
200
400
H, Oe
YBCO
T = 77.4K
H ⊥ I
H ∥ I
θ = 80⁰, 70⁰,...20⁰, 10⁰
from top to bottom

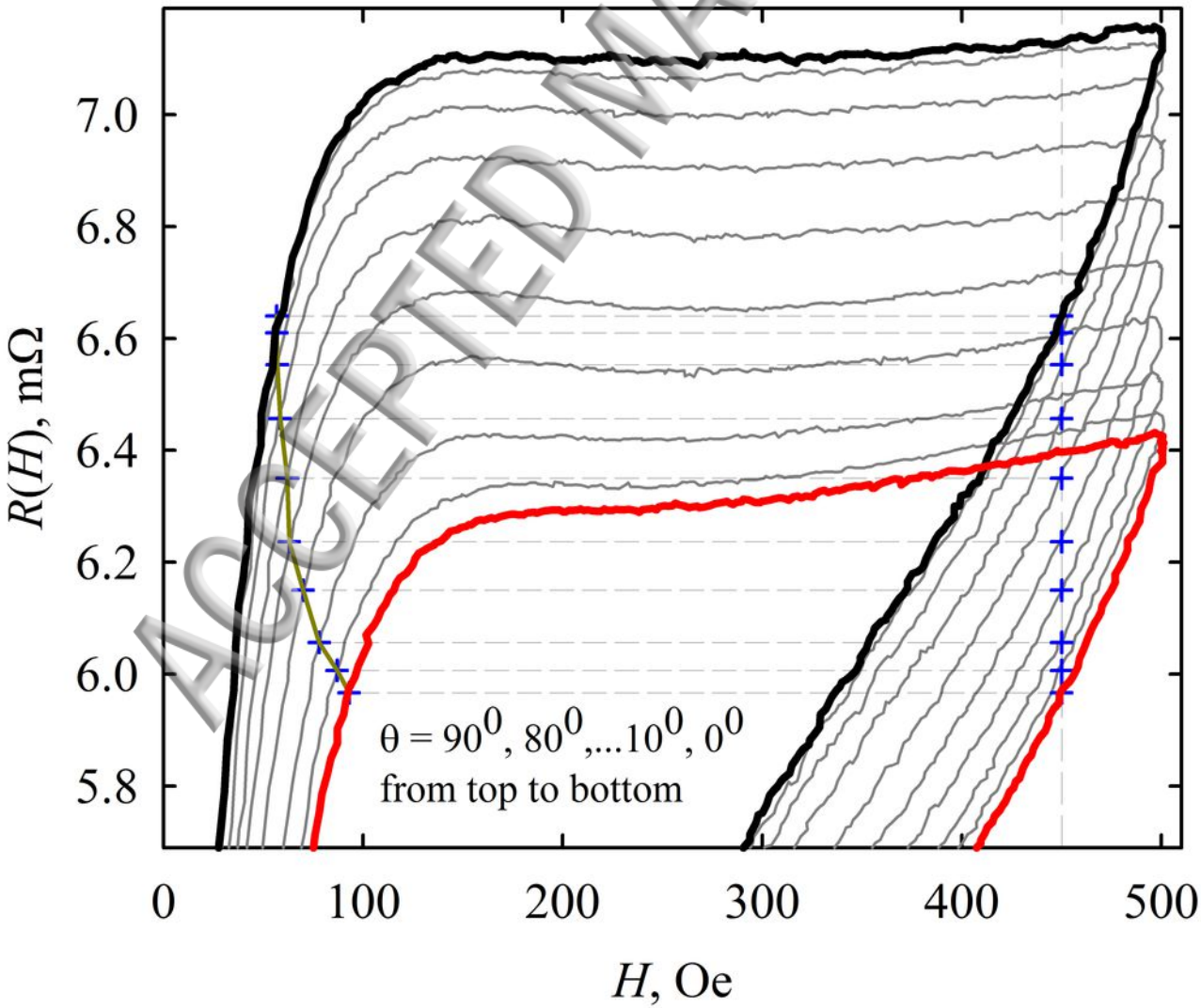
7.0
6.8
6.6
6.4
6.2
6.0
5.8
R(H), mΩ
0
100
200
300
400
500
H, Oe
θ = 90⁰, 80⁰,...10⁰, 0⁰
from top to bottom

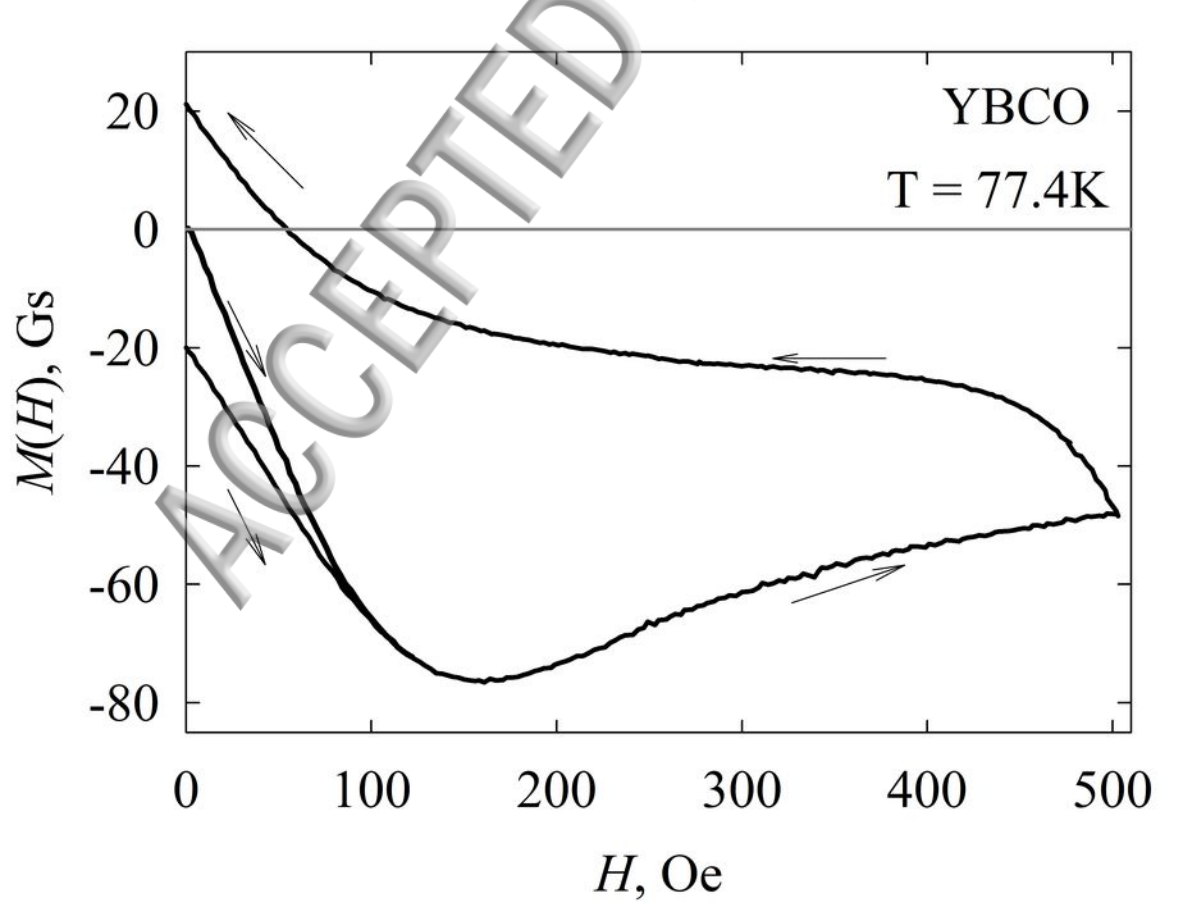

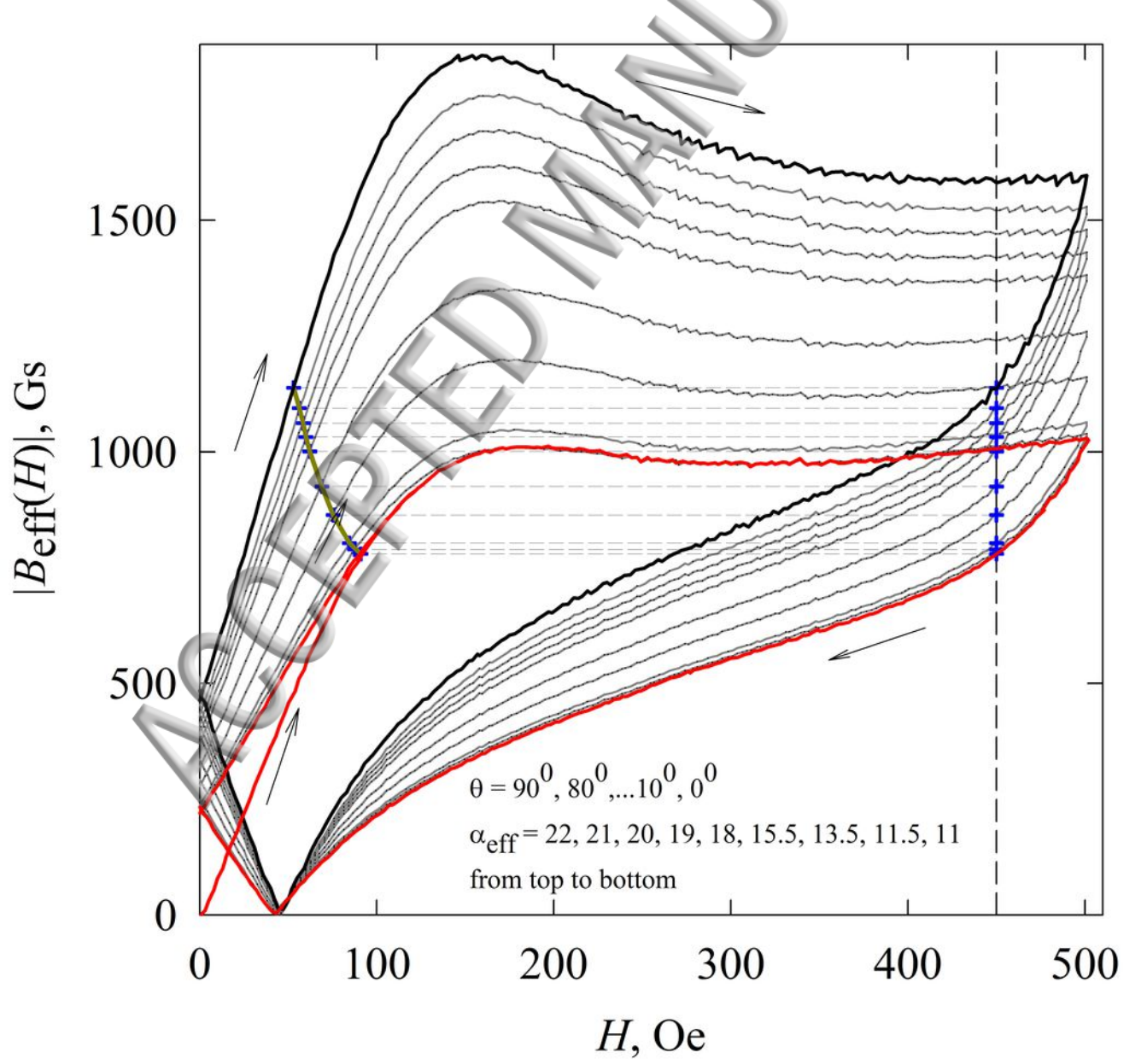

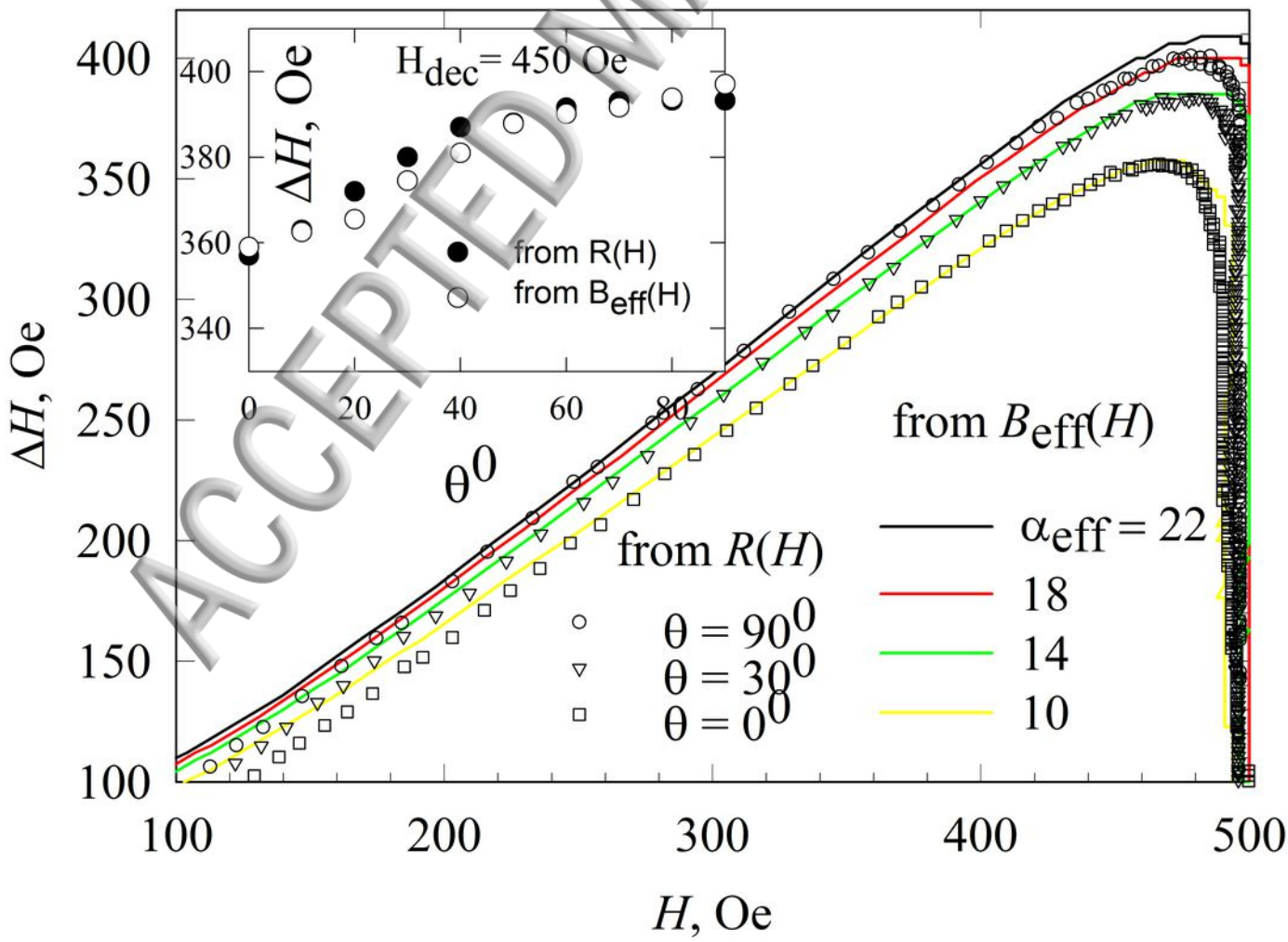
ΔH, Oe
H, Oe
100
150
200
250
300
350
400
100
200
300
400
500
from $B_{eff}(H)$
α_{eff} = 22
18
14
10
from $R(H)$
θ = 90⁰
θ = 30⁰
θ = 0⁰
H_{dec} = 450 Oe
ΔH, Oe
from R(H)
from B_{eff}(H)
θ⁰
0
20
40
60
80
340
360
380
400

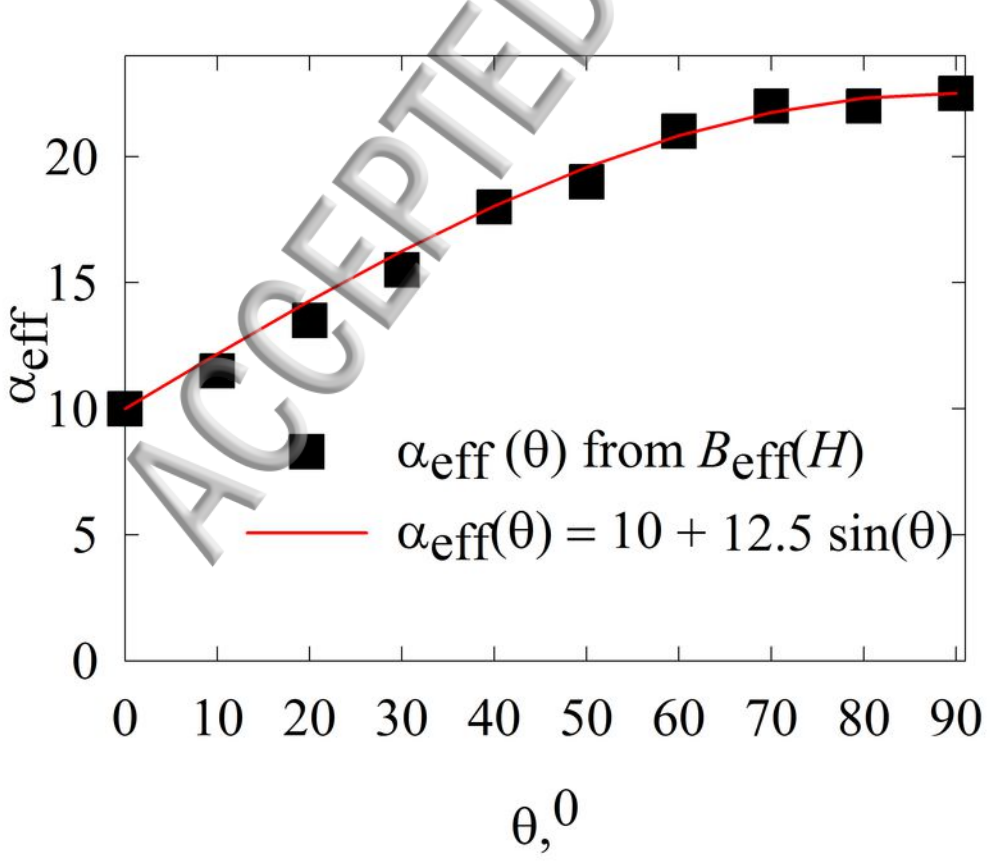
ACCEPTED
20
15
10
5
0
α_{eff}
α_{eff} (θ) from $B_{eff}(H)$
$\alpha_{eff}(\theta) = 10 + 12.5 \sin(\theta)$
0 10 20 30 40 50 60 70 80 90
θ, ^{0}